Surface de section dans le problème de Störmer,

par René DE VOGELAERE (*)
Docteur en Sciences mathématiques
Associate Professor University of Notre Dame -Ind.

Résumé. — L'auteur se propose de préciser et de compléter des résultats obtenus par Graef et par Godart, dont certains n'ont pas été publiés explicitement, et relatifs à la façon dont il est possible d'introduire une surface de section au sens de Poincaré dans le problème de Störmer. Il donne en particulier une démonstration directe de la conjecture de Godart suivant laquelle toute trajectoire rencontre une fois au moins l'équateur ou le thalweg.

1. INTRODUCTION. Si toutes les trajectoires d'un problème de dynamique à deux degrés de liberté rencontrent une surface, Poincaré l'appelle surface de section [6]. Une telle surface peut être obtenue dans le problème de Störmer à partir d'une proposition de Graef [3], que nous indiquons ci-dessous par P^2. Graef a ramené la démonstration de P^2 à celle d'une conjecture due à Godart. Nous nous proposons ici, après avoir rappelé les équations différentielles du problème, de préciser diverses propositions de l'article de Graef, de donner une démonstration directe de P^2 et d'en déduire ensuite une surface de section du problème.

2. ÉQUATIONS DIFFÉRENTIELLES DU PROBLÈME. Dans le problème de Störmer, on étudie le mouvement d'une particule électrisée dans le champ d'un dipôle magnétique élémentaire ; ce mouvement peut être décomposé en celui du plan méridien qui suit la particule et celui dans le plan méridien [4], on met ainsi en évidence un paramètre γ_1, cependant seules les valeurs positives de γ_1 sont intéressantes et dans ce cas les équations du mouvement dans le plan méridien sont données par

$$\begin{aligned} \ddot{x} &= \partial U / \partial x \\ \ddot{\lambda} &= \partial U / \partial \lambda \end{aligned} \tag{2.1}$$

(*) Présenté par M. le Chanoine G. LEMAÎTRE.

avec

(2.2) $$\dot{x}^2 + \dot{\lambda}^2 = 2U = (2\gamma_1)^{-4} e^{2x} - (e^{-x}\cos\lambda - 1/\cos\lambda)^2,$$

les dérivations se faisant par rapport à une variable σ étroitement liée au temps, λ étant la latitude et $r = e^x/2\gamma_1$ étant la distance au dipôle ; $\lambda = 0$ représente donc l'intersection du plan méridien avec l'équateur géomagnétique. La ligne

$$e^{-x} - 1/\cos^2\lambda = 0$$

qui joue un certain rôle dans la suite est connue sous le nom de thalweg.

3. Propositions de Godart-Graef. Nous considérerons uniquement les trajectoires dans le plan méridien ; la ligne $\lambda = 0$ sera appelée l'équateur, sur cette ligne se trouvent des trajectoires [7] que nous excluons dans ce qui suit ; quand nous parlons de trajectoires qui s'en vont à l'infini, nous avons en vue l'infini positif, les trajectoires qui ne sont pas bornées pour x négatif correspondent aux trajectoires par le dipôle élémentaire [8] qui est d'ailleurs sur le thalweg.

Réécrivons maintenant quelques-unes des propositions de Graef :

P^1 : Toutes les trajectoires rencontrent une fois au moins l'équateur ou le thalweg. [3, p. 11, Th. III].

P^2 : Si $\gamma_1 > 0$, toutes les trajectoires rencontrent l'équateur, sont asymptotiques à l'équateur ou s'en vont à l'infini. [3, p. 28, Th. V et premier paragraphe p. 26],

P^3 : Si $\gamma_1 \geq 1$, toutes les trajectoires rencontrent l'équateur ou sont asymptotiques à cette ligne [3, p. 30, Th. VII et convention p. 28, Th. V].

4. Commentaires. P^1 est la conjecture de Godart ; une partie de la démonstration est contenue dans des notes non publiées par lui et Graef se contente de dire qu'il est possible de démontrer aisément P^1 au moyen de la figure 4 de son article. La chose n'est pas aussi simple, nous n'en donnerons qu'une démonstration schématique ; celle-ci se fait le mieux si on utilise les coordonnées

$$\xi = e^x \cos\lambda, \quad \eta = e^x \sin\lambda, \quad dt = e^{2x} d\sigma,$$

donnant les équations

$$\ddot{\xi} = \frac{\partial P}{\partial \xi}, \quad \ddot{\eta} = \frac{\partial P}{\partial \eta}$$

$$\dot{\xi}^2 + \dot{\eta}^2 = 2P = (2\gamma_1)^{-4} + (\xi r^{-3} - \xi^{-1})^2$$

avec $r^2 = \xi^2 + \eta^2$, les dérivations se faisant par rapport à t.

a) Une solution $\eta =$ constante, n'est possible que si la constante est nulle.

b) Si partant d'un point dans la direction des t croissants (ou décroissants), $\dot{\eta}$ garde un signe constant et que la solution est bornée, η tend vers une limite et celle-ci doit être nulle ; donc, si la solution est bornée dans une direction de t, ou $\dot{\eta}$ s'annule indéfiniment souvent, ou la solution est asymptotique à $\eta = 0$; dans le premier cas $\ddot{\eta}$ s'annule à cause du théorème de Rolle ce qui n'arrive que sur l'équateur ou le thalweg ($\partial P / \partial \eta = 0$).

c) Si la solution n'est pas bornée dans les deux directions de t, ni asymptotique à l'équateur pour ξ infini et que η est constamment positif, $\dot{\eta}$ tend vers une limite positive quand t tend vers $+ \infty$, négative quand t tend vers $- \infty$, la courbe a donc un minimum ($\partial P / \partial \eta > 0$) et donc doit traverser le thalweg.

P^2 est la proposition essentielle et pour la démontrer, Graef utilise P^1 et prouve que toute trajectoire coupant le thalweg rencontre nécessairement l'équateur ou s'en va à l'infini, il lui faut pour cela étudier l'allure des trajectoires au voisinage d'un point de rencontre avec le thalweg et montrer ensuite qu'une courbe ne peut rencontrer indéfiniment le thalweg sans rencontrer l'équateur ou être asymptotique à cette ligne.

Pour démontrer P^3, qui précise P^2 pour les valeurs indiquées de γ_1, il remarque que dans ces conditions les trajectoires se trouvent dans l'une ou l'autre de deux régions non connexes, l'une est bornée en coordonnées ξ, η, et le thalweg est entièrement exclu de l'autre.

Nous démontrerons maintenant P^2 directement tout en précisant l'énoncé.

5. COORDONNÉES DE LEMAITRE-BOSSY. Lemaître et Bossy [5] ont défini de nouvelles coordonnées u, y par

$$x = 2 \log \cos y + u \cos v \tag{5.1}$$
$$\lambda = y + u \sin v$$

v étant lié à y par $\operatorname{tg} v = 2 \operatorname{tg} y$.

Les formules (5.1) établissent une correspondance biunivoque entre les demi-plans $\lambda > 0$ et $y > 0$, car une telle correspondance existe pour les points du thalweg ($u = 0$, $y = \lambda$) et que

$$J = \frac{D(x, \lambda)}{D(u, y)} = \frac{1}{\cos v}\left(1 + 2u \frac{\cos^3 v}{\cos^2 y}\right) > 0, \tag{5.2}$$

si on a

$$\lambda > 0 \quad \text{et} \quad y > 0. \tag{5.3}$$

Cette dernière relation se montre aisément car de la condition (5.3) qui peut s'écrire

$$u > -y/\sin v,$$

on déduit

$$1 + 2u \frac{\cos^3 v}{\cos^2 y} > 1 - \frac{2y \cos^3 v}{\sin v \cos^2 y} = 1 - \frac{y}{\operatorname{tg} v} \cdot \frac{1}{1 + 3 \sin^2 y} > 0.$$

D'autre part,

a) si $u < 0$, on déduit de (5.1)

$$x < 2 \log \cos y, \ \lambda < y \text{ et donc } e^{-x} - 1/\cos^2 \lambda > 0 ;$$

b) si $u > 0$, il faut inverser tous les signes d'inégalités.

6. PROPRIÉTÉS DES ÉQUATIONS DU MOUVEMENT EN COORDONNÉES u, y.

En dérivant les équations (5.1) on trouve

$$\dot{x} = (-\dot{y} \sin v + \dot{\lambda} \cos v)/J$$

et si $\dot{y} = 0$,

$$\ddot{y} = (-\ddot{x} \sin v + \ddot{\lambda} \cos v)/J ;$$

nous montrerons maintenant que si $y = 0$, $\dot{y} < 0$, c'est-à-dire que

$$A = \ddot{x} \operatorname{tg} v - \ddot{\lambda} > 0.$$

Remplaçons pour cela dans A, $\ddot{x}$ et $\ddot{\lambda}$ par leur valeur déduite des équations du mouvement (2.1), on a

$$A = (e^{2x}/16\gamma_1^4 - e^{-x} + e^{-2x}\cos^2\lambda)\operatorname{tg} v + [(1/\cos^2\lambda) - e^{-2x}\cos^2\lambda]\operatorname{tg}\lambda.$$

Si on pose

$$B = e^{-x} - 1/\cos^2\lambda$$

et

$$C = 2e^{-x}\cos^2\lambda \operatorname{tg} y - (1 + e^{-x}\cos^2\lambda)\operatorname{tg}\lambda,$$

on voit que $A - BC = e^{2x}\operatorname{tg} v/16\gamma_1^4 > 0$.

a) Si $u < 0$, $B > 0$ et $C > 2e^{-x}\cos^2\lambda \operatorname{tg} y - (e^{-x}\cos^2\lambda + 1)\operatorname{tg} y$, donc $C > (e^{-x}\cos^2\lambda - 1)\operatorname{tg} y > 0$;

b) si $u > 0$, $B < 0$ $C < 2e^{-x}\cos^2\lambda \operatorname{tg}\lambda - (e^{-x}\cos^2\lambda + 1)\operatorname{tg}\lambda$, donc $C < (e^{-x}\cos^2\lambda - 1)\operatorname{tg}\lambda < 0$.

Dans chaque cas, $BC > 0$ et donc $A > 0$.

7. Démonstration de P^2. La section précédente nous montre que si une trajectoire a un extremum en $\ddot{y}$ ($\dot{y} = 0$) pour $y > 0$, ce ne peut être qu'un maximum ($\ddot{y} < 0$).

Considérons une trajectoire ayant un point $P(\sigma_0)$ tel que $y > 0$; toute trajectoire pouvant être parcourue dans les deux sens on choisira celui qui sera tel que si $\sigma > \sigma_0$, $\dot{y}(\sigma) < 0$ tant que $y > 0$.

Si la trajectoire peut sortir d'un domaine borné, u tendra vers l'infini et y vers zéro.

Si la trajectoire reste dans un domaine borné, comme $y(\sigma) = 0$ ne peut être minimum pour σ fini (car $y = 0$ et $\dot{y} = 0$ implique $y \equiv 0$), ou bien $y(\sigma)$ diminuera jusqu'à atteindre des valeurs négatives, ou bien $y(\sigma)$ tendra vers zéro à cause de (5.1) quand σ tendra vers l'infini ; dans ce dernier cas la trajectoire serait asymptotique à une trajectoire périodique pour laquelle $y \equiv 0$.

Mais nous avons étudié le voisinage des solutions périodiques [2] et montré pour quelles valeurs de γ_1 ces orbites sont stables ou instables ; dans chaque cas les orbites voisines rencontrent

$\lambda = 0$, après un temps suffisamment long ; cela est évident pour les orbites stables et aussi pour les orbites instables impaires ($\cosh \Omega T - 1$) pour lesquelles les orbites voisines rencontrent l'orbite périodique un nombre impair de fois à chaque période, mais il en est ainsi également pour les orbites instables paires ($\cosh \Omega T > 1$) car des solutions particulières dites paire ou impaire s'annulent à chaque période au moins deux fois et il en est alors de même de toute solution à cause du théorème de Sturm.

Ceci démontre directement la proposition suivante plus précise que P^2 :

P^4 : *Si* $\gamma_1 > 0$, *toute trajectoire qui ne se trouve pas sur la droite* $\lambda = 0$, *rencontre cette droite ou s'en va à l'infini.*

8. EXEMPLE D'ORBITE NE RENCONTRANT PAS $\lambda = 0$. Il résulte aussi de ce qui précède que P^3 peut être précisé par

P^5 : *Si* $\gamma_1 \geq 1$, *toutes les trajectoires rencontrent l'équateur.*

Il se pourrait même que le domaine de γ_1 dans cet énoncé puisse être étendu à des valeurs plus petites que un, mais de toute façon il y a une limite inférieure. En effet, Störmer a montré que les trajectoires par le dipôle élémentaire ne rencontre plus l'équateur dès que γ_1 est suffisamment petit, par interpolation de ses résultats [8] on trouve comme limite $\gamma_1 = 0.47$, l'orbite correspondante, passe par le dipôle et est asymptotique à l'infini à $\lambda = 0$. Nous montrerons à présent qu'il existe des orbites ne rencontrant pas l'équateur pour des valeurs de γ_1 plus grandes que 0.47 (voisines de 0.78). L'exemple est en lui-même assez instructif.

Sur $\lambda = 0$, on sait que les équations (2.1) et (2.2) s'intègrent au moyen des fonctions elliptiques ; en particulier, si $0 < \gamma_1 < 1$ et qu'on pose

$$a_0^2 = (2\gamma_1)^{-2}, \quad b_0^2 = (\gamma_1^{-2} - 1)/4 \quad \text{et} \quad c_0^2 = (\gamma_1^{-2} + 1)/4,$$

on vérifie aisément que

$$(2\gamma_1 r)^{-1} = z = e^{-x} = \frac{1}{2} + c_0 cn a_0, \quad \lambda = 0$$

est solution de (2.2).

La fonction *cn* de Jacobi doit être calculée pour le module $k = c_0/a_0$. Les points réels sur l'orbite ont lieu pour $r > 0$, donc $z > 0$ et $cna_0 > -(2c_0)^{-1}$, tandis que le point à l'infini correspond à $cna_0 = -(2c_0)^{-1}$.

Les orbites au voisinage de cette orbite équatoriale se calculent au moyen des équations aux variations, voir par exemple [2]. La variation dite paire est celle qui correspond à une orbite partant au voisinage de minimum en x de l'orbite équatoriale avec les valeurs initiales $\Delta\lambda = 1$ et $\Delta\dot{\lambda} = 0$, or si nous choisissons $k^2 = 0.8$ ce qui correspond à $\gamma_1 = 0.77460$, nous obtenons à quatre décimales les chiffres du tableau ci-joint, la première colonne indiquent les valeurs de $z = e^{-x}$ sur l'orbite équatoriale et la seconde la variation paire. Pour x infini, celle-ci vaut 0.0789, L'orbite variée ne rencontre donc pas l'équateur à distance finie et il existe donc au voisinage de l'équateur des orbites venant de l'infini passant par un minimum en x et rebroussant chemin sans jamais rencontrer $\lambda = 0$. Le même calcul répété pour les diverses valeurs de γ_1 montrerait probablement qu'il en est ainsi pour toutes les valeurs de γ_1 positives mais plus petite qu'une certaine valeur un peu supérieure à 0.78, pour laquelle l'orbite en question est asymptotique à l'infini.

$z = e^{-x}$	$\cong \lambda$
1.3165	1.0000
1.2593	1.0607
1.1253	1.2250
0.9526	1.4427
0.7931	1.6371
0.6401	1.7283
0.5000	1.6489
0.3599	1.3633
0.2069	0.8805
0.0474	0.2582
— 0.1253	— 0.4067
— 0.2593	— 1.0055
— 0.3165	— 1.4478

. **9.** SURFACE DE SECTION. Nous en arrivons maintenant à l'application des considérations que nous venons de faire à la recherche de la surface de section.

Réunissons d'abord quelques notations utiles :

$$g = \log [2\gamma_1(\sqrt{\gamma_1^2 + 1} - \gamma_1)] \qquad g_1 = \log [2\gamma_1(\gamma_1 - \sqrt{\gamma_1^2 - 1})]$$

$$g_2 = \log [2\gamma_1(\gamma_1 + \sqrt{\gamma_1^2 - 1})] \qquad f = \log (2\gamma_1^{4/3})$$

$$m(h) = \arccos [2^{-3}e^{2h}(\sqrt{\gamma_1^{-2} + 64e^{-3h}} - \gamma_1^{-1})].$$

La discussion dépend des régions du plan (U = 0) dans lesquelles peuvent se trouver les trajectoires ; la forme de ces régions a été étudiée par Störmer et est représentée en coordonnées x, λ sur la figure 7 d'un article de Vallarta [9].

a) Si $0 < \gamma_1 < 1$, la région $U > 0$ est simplement connexe et s'étend à l'infini, elle contient la portion de l'axe des x à droite de $x = g$; de P[4] nous déduisons que toutes les trajectoires situées dans le domaine $U > 0$, $\lambda > 0$, $x < h$, auront comme ligne de section l'ensemble des deux segments

$$\lambda = 0 \quad g \leq x \leq h,$$
$$x = h \quad 0 \leq \lambda \leq m(h),$$

le point $(h, m(h))$ étant sur la frontière $U = 0$.

b) Si $\gamma_1 \geq 1$, la région $U > 0$ est doublement connexe, une des sous-régions ne s'étend pas vers l'infini positif des x et contient une portion de l'axe des x bornée à gauche par $x = g$, à droite, par $x = g_1$, les trajectoires de cette région admettrons d'après P[5] l'axe des x comme ligne de section ou plus précisément le segment

$$\lambda = 0 \quad g \leq x \leq g_1.$$

L'autre sous-région s'étend à l'infini et contient la portion de l'axe des x bornée à gauche par $x = g_2$ elle admet comme ligne de section l'axe des x ou plus précisément le segment

$$\lambda = 0 \quad g_2 \leq x.$$

10. QUELQUES REMARQUES. Comme l'établissement d'une surface de section est surtout utile pour l'étude des orbites périodiques, nous rappelons les résultats sur les orbites périodiques obtenus en [1], à savoir,

T¹. Les orbites périodiques se trouvent entièrement à gauche de la droite $x = f$.

T². Toute orbite périodique rencontre l'axe des x sur le segment $g \leq x \leq f$.

On en déduit, si $\gamma_1 \geq 1$, que seule la première sous-région contient des orbites périodiques puisque $f < g_2$; seule la ligne de section correspondante sera importante.

D'autre part, si $0 < \gamma_1 < 1$, il n'y aura d'orbites périodiques que si $f > g$, c'est-à-dire que si $\gamma_1 > \sqrt{2}/4$ [1] ; ceci donne une limite inférieure pour la borne inférieure c des valeurs de γ_1 pour lesquelles existent des orbites périodiques. On voit aussi que si h est choisi plus grand que f, toute orbite périodique rencontre la ligne de section sur le segment de l'axe des x.

De ces résultats, on déduit une surface de section pour le problème dans l'espace, qui sera la surface de révolution autour de l'axe du dipôle ayant pour génératrice la ligne de section en coordonnées r, λ déduite de la ligne de section ci-dessus, obtenue en coordonnées x, λ (¹).

Université Notre Dame,
Notre Dame, Ind., États-Unis.

BIBLIOGRAPHIE

1. R. DE VOGELAERE, Non existence d'orbites périodiques dans le problème de Störmer pour certaines valeurs du paramètre, *Ann. Assoc. Canad. Franç. Avanc. Sci.*, Univ. Montréal, 1952.

2. R. DE VOGELAERE, Équation de Hill et Problème de Störmer. *Can., Journal Math.*, 2, 440-456, 1950.

(¹) Ces recherches ont été partiellement subventionnées par le « United States Air Force » par l'intermédiaire de l'« Office of Scientific Research of the Air Research and Development Command ».

3. C. GRAEF, Orbitas periodicas de la radiacion cosmica primaria, *Bol. Soc. Matem. Mexicana*, **1**, 1-31, 1944.

4. G. LEMAÎTRE, Champ magnétique et rayons cosmiques, *Ciel et Terre*, Bruxelles, **59**, 1-16 1943.

5. G. LEMAÎTRE et L. BOSSY, Sur un cas limite du problème de Störmer, *Ac. Roy. Belg.*, **31**, 357-364, 1945.

6. H. POINCARÉ, Les méthodes nouvelles de la mécanique céleste. Vol. 3, Paris 1899,

7. C. STÖRMER, Sur les trajectoires des corpuscules électrisés dans l'espace sous l'action du magnétisme terrestre, *Arch. Sci. Phys. et Nat.*, Genève, **24**, 350-357, 1907.

8. C. STÖRMER, Résultats de Calculs numériques. I Trajectoires par l'origine. *Vid. Selsk. Skrifter. Mat.-naturv.* Klasse 1913, n° 4.

9. M. VALLARTA, An outline of the allowed cone of cosmic radiation. *Univ. of Toronto.* Publ., 1-56, 1938.

TRANSFER MAP APPROACH TO THE BEAM-BEAM INTERACTION

Alex J. Dragt

Los Alamos Scientific Laboratory, Los Alamos, New Mexico 87545

and

University of Maryland, College Park, Maryland 20742

ABSTRACT

A study is made of a model for the beam-beam interaction in ISABELLE using numerical methods and the recently developed method of Transfer Maps. It is found that analytical transfer map calculations account qualitatively for all the features of the model observed numerically, and show promise of giving quantitive agreement as well. They may also provide a kind of "magnifying glass" for examining numerical results in fine detail to ascertain the presence of small scale stochastic motion that might lead to eventual particle loss. Preliminary evidence is presented to the effect that within the model employed, the beam-beam interaction at its contemplated strengths should not lead to particle loss in ISABELLE.

I. INTRODUCTION

The purpose of this paper is to explore the model of Herrera, Month, and Peierls[1] for the ISABELLE beam-beam interaction with the aid of the recently developed method of Transfer Maps[2] and its associated Lie algebraic techniques.[3] The model employed for the beam-beam interaction is "weak-strong".[1,4] One beam, the strong beam, is taken to be fixed, and the other beam, the weak beam, is treated as a collection of particles that are affected by their passage through the strong beam but not by each other. The strong beam is assumed to be an unbunched ribbon in the horizontal plane whose vertical charge distribution is well described by a Gaussian shape. The weak beam also lies in the same horizontal plane and crosses the strong beam at a fixed angle. Only vertical deflections of the weak beam by the strong beam are taken into account.

In the strong beam-weak beam limit, the net motion of a particle in the weak beam can be viewed as the continual repetition of two sequential motions: passage through the storage ring followed by passage through the strong beam. (See Fig. 1.) The equations of motion for each of these two passages (through the ring and through the strong beam) are derivable from Hamiltonians, and therefore each passage is described by a symplectic (Poisson bracket preserving) transfer map.[2,3]

By design, the passage through a storage ring is well described by a linear map. Upon restricting attention only to vertical motion and making a suitable choice of coordinates, the "ring" transfer map can be written as

$$\begin{aligned} q' &= q\cos(2\pi w) + p\sin(2\pi w) \\ p' &= -q\sin(2\pi w) + p\cos(2\pi w). \end{aligned} \tag{1}$$

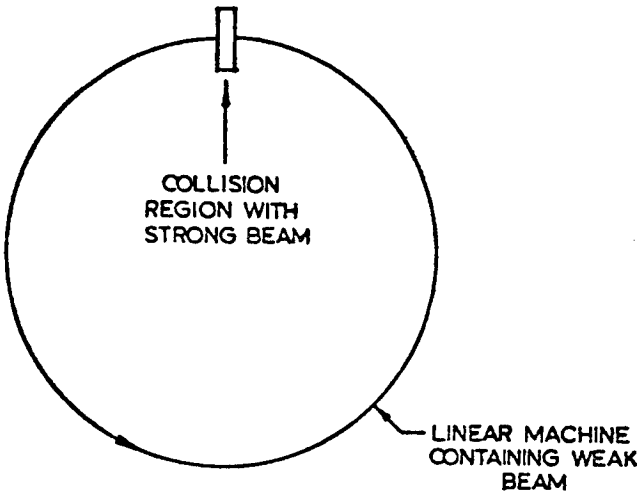

Fig. 1. Schematic representation of particle motion in a storage ring and a colliding beam region.

Here q is proportional to the vertical coordinate of a particle in the weak beam, p is a suitably chosen canonically conjugate momentum, and w (modulo an integer) is the tune of the storage ring.[1] The unprimed variables q,p specify the particle orbit just as it enters the ring, and the primed variables q',p' describe the orbit upon exit.

The effect of passage through the strong beam is more complicated. To find the "beam" transfer map exactly, it is necessary to integrate the nonlinear equations of motion for a particle passing through the strong beam. However, a good approximation to this map is given by assuming that the particle suffers a vertical momentum change depending only upon its initial vertical position, and that the vertical position itself remains unaffected:

$$q'' = q'$$
$$p'' = p' + u(q'). \tag{2}$$

This impulse approximation becomes exact in the limit that the interaction region becomes a point and/or the transit time through the region approaches zero. In any case, the beam mapping (2) is symplectic, and therefore its use will produce no qualitative error.

The function u is proportional to the electrostatic force exerted by the strong beam. In the coordinates and Gaussian model employed, u is given by the relation[1]

$$u(q) = 4\pi D/\sqrt{3} \int_0^{q\sqrt{3}} dt\, e^{-t^2}. \tag{3}$$

Here D is the beam-beam strength parameter that typically[4] has values ranging from 10^{-3} to 10^{-2}. It is normalized in such a way that the beam-beam interaction depresses the tune for infinitesimal betatron oscillations by an amount D when D is small.

There is one last caveat to be made. According to the current design, ISABELLE will actually have 6 collision regions separated by 6 identical lattice sections. Thus, in reality, the maps 1 and 2 must be iterated 6 times to simulate the effect of one complete turn. Correspondingly, Eq. (1) is the transfer map for one lattice section and w (modulo an integer) is actually 1/6 of the total machine tune.

In this paper the effect of repeated iteration of the maps (1) and (2) are studied using Transfer Map methods and results are compared with numerical calculations.

II. TRANSFER MAP RESULTS

To treat q and p on an equal footing, it is notationally convenient to introduce variables z_1 and z_2 by the relations

$$z_1 = q$$
$$z_2 = p. \tag{4}$$

Employing this notation, let f(z) be any function of the phase-space variables z. With each such function f these is an associated Lie operator F. This operator acts on functions and is defined by the rule

$$Fg = [f,g]. \tag{5}$$

Here g is any function of the phase-space variables, and the square bracket [,] denotes the Poisson bracket operation familiar from classical mechanics.

Next, consider the object exp(F), called a Lie transformation, defined by the exponential series

$$\exp(F) = I + F + F^2/2! + F^3/3! + \ldots. \tag{6}$$

More explicitly, the action of exp(F) on an arbitrary function g is given by the expression

$$\exp(F)g = g + [f,g] + [f,(f,g)]/2! + \ldots. \tag{7}$$

Now consider the operator $\exp(F_2)$ where F_2 is the Lie operator associated with the quadratic polynomial

$$f_2 = -\pi w(z_1^2 + z_2^2). \tag{8}$$

It is easily verified that

$$F_2 z_1 = [f_2, z_1] = 2\pi w z_2$$
$$F_2 z_2 = [f_2, z_2] = -2\pi w z_1. \tag{9}$$

Consequently, use of (7) and (9) gives the relation

$$\exp(F_2)\ z_1 = z_1 + z_2(2\pi w) - z_1(2\pi w)^2/2! - z_2(2\pi w)^3/3! + \ldots = z_1 \cos(2\pi w) + z_2 \sin(2\pi w). \tag{10a}$$

Similarly, it can be checked that

$$\exp(F_2)\ z_2 = -z_1 \sin(2\pi w) + z_2 \cos(2\pi w). \tag{10b}$$

Therefore the ring transfer map (1) can be written in the compact form

$$z' = \exp(F_2)\ z. \tag{11}$$

A similar Lie transformation representation can be found for the beam transfer map (2). Let $f_b(z)$ be the function defined by the relation

$$f_b(z) = \int_0^z 1\ u(q)\ dq. \tag{12}$$

The Poisson bracket relations analogous to (9) are

$$F_b\ z_1 = [f_b, z_1] = 0$$
$$F_b\ z_2 = [f_b, z_2] = -\partial f_b/\partial z_1 = u(z_1) \tag{13}$$
$$F_b^2\ z_2 = [f_b, (f_b, z_2)] = [f_b, u(z_1)] = 0, \text{ etc.}$$

Consequently the infinite sum (7) is trivial to evaluate in this case because it terminates. One finds the result

$$\exp(F_b)\ z_1 = z_1$$
$$\exp(F_b)\ z_2 = z_2 + u(z_1). \tag{14}$$

Therefore the beam transfer map (2) can be written in the form

$$z'' = \exp(F_b)\ z'. \tag{15}$$

Combing the two results (11) and (15), one finds that the net transfer map M for passage through the ring followed by passage through the strong beam is given by the product

$$M = \exp(F_2)\ \exp(F_b). \tag{16}$$

The observant reader may be worried about the order in which the two factors appear in (16). It can be verified that the above order indeed is correct because Lie transformations have the property

$$\exp(F_2)\ g(z) = g\ \exp(F_2)\ z = g(z') \tag{17}$$

for any function $g(z)$.[3]

The problem at hand is to evaluate M^n for large n in order to compute the effect of many passages through the ring and the strong beam. The computation of M^n would be easy if a Lie operator H could be found such that M could be reexpressed in the form $\exp(H)$, for then M^n would be simply given by $\exp(nH)$. The determination of such an H is a standard problem in the theory of Lie algebras that is solved by using the Campbell-Baker-Hausdorff formula.[3] This formula gives H in terms of F_2 and F_b, and their multiple commutators. In addition, there is an analogous formula that gives the function h associated with H in terms of f_2 and f_b, and their multiple Poisson brackets. It also can be shown that the computation of $\exp(nH)$ is equivalent to the integration of a "trajectory" in "z space" for n units of "time" using -h as an "effective" Hamiltonian. Consequently, the function h(z) is formally invariant under the map. This means that the function h(z) generalizes the Courant-Snyder invariant to the case of nonlinear motion.

For the problem under consideration, h is given by the formal operator formula,

$$h = f_2 + F_2\,[1 - \exp(-F_2)]^{-1}\ f_b + \ldots. \tag{18}$$

The terms not shown in the series involve Poisson brackets with more than one f_b, and therefore are quadratic and higher order in the beam-beam strength parameter. Consequently, as it stands, Eq. (18) is correct through first order in the beam-beam strength.

The computation of the effect of the operator F_2 and the functions of F_2, such as occur in (18), is facilitated by the introduction of "polar" coordinates in phase space and the use of Fourier series. This can be achieved in a canonical way by using action angle variables a, Φ defined by the relations

$$\begin{aligned} q = z_1 &= (2a)^{\frac{1}{2}} \sin \Phi \\ p = z_2 &= (2a)^{\frac{1}{2}} \cos \Phi. \end{aligned} \tag{19}$$

It is evident from (5) and (8) that F_2 annihilates any function of a. By contrast, use of (1), (11), and (17) shows that

$$\exp(F_2)\, a^{n/2} \exp(in\hat{\Phi}) = \exp(i2\pi\pi w)\, a^{n/2} \exp(in\hat{\Phi}). \tag{20}$$

Consequently, the functions $\exp(in\hat{\Phi})$ are eigenfunctions of F_2 with eigenvalues $i2\pi\pi w$:

$$F_2 \exp(in\hat{\Phi}) = i2\pi\pi w \exp(in\hat{\Phi}). \tag{21}$$

This result can also be obtained by direct evaluation of the Poisson bracket $[f_2, \exp(in\hat{\Phi})]$.

The determination of h as given in (18) is now straightforward. Inserting (19) into (12) and making a Fourier expansion, one finds

$$f_b = \sum_{-\infty}^{\infty} c_n(a) \exp(i2n\hat{\Phi}) \tag{22}$$

where

$$c_n = 4\pi Da \int_0^1 \int_0^1 du\, dv\, v \exp(-3au^2v^2) \times [I_n(3au^2v^2) - I_n'(3au^2v^2)]. \tag{23}$$

Here the symbols I_n denote modified Bessel functions, and use has been made of the standard relations[5]

$$\exp(x \cos y) = \sum_{-\infty}^{\infty} I_n(x) \exp(iny) \tag{24a}$$

$$I_{n+1} + I_{n-1} = 2I_n'. \tag{24b}$$

Now insert (22) into (18) and use the eigenfunction property (21). The result is that h is given in complex form by the expression,

$$h = -2\pi wa + \sum_{-\infty}^{\infty} c_n(a) [2\pi\pi w/\sin(2\pi\pi w)] \exp[2in(\hat{\Phi} + \pi w)], \tag{25a}$$

and in real form by the expression,

$$h = -2\pi wa + c_o(a) + 2 \sum_{1}^{\infty} c_n(a) [2\pi\pi w/\sin(2\pi\pi w)] \cos[2n(\hat{\Phi} + \pi w)]. \tag{25b}$$

The expressions (25) provide a generalization of the Courant-Snyder invariant through first order in the beam-beam interaction strength. Upon inspecting them, several points are immediately evident:

(a) Resonances occur and the formulas diverge whenever the tune w is of the form

$$w = k/(2N) \tag{26}$$

where k and N are integers. Thus there are resonances at half-integer tunes, quarter-integer tunes, sixth-integer tunes, etc. This was to be expected because u(q) as given by (3) contains no even powers and all odd powers of q.

(b) The strengths of the various order resonances are proportional to $nc_n(a)$. Using the large n expansion,[5]

$$I_n(x) \sim \exp[-n \log(2n/ex)], \tag{27}$$

one finds from (23) that the strengths of the various resonances fall off faster than exponentially as n is increased. Therefore the sizes of various resonance features in phase space should decrease in size according to their proximity to the origin in phase space.

It also follows that (25) converges rapidly at all tune values for which w is badly approximated by rationals. Indeed, the points in tune space where (25) fails to converge are of measure zero.[6]

(c) With the aid of time reversal invariance it can be shown from (16) that the locations of various features in phase space as fixed points and separatrices must be symmetric about the line $\Phi = \pi/2 - \pi w$ for all beam-beam interaction strengths. (Note that according to (19), the line $\Phi = 0$ corresponds to the p axis.) Because f_b as given by (12) is even in z_1, there is also symmetry in phase with respect to inversion through the origin. Examination of (25) shows that both of these symmetries are present in h.

To calculate the behavior of M exactly at and near resonance, it is necessary to work with powers of M. For example, consider m'th order resonances. Then m = 2N and tunes near an m'th order resonance value can be written in the form

$$w = k/m + \delta \tag{28}$$

where δ measures departure from exact resonance. Moreover, it can be shown that there is a Lie operator H_r such that M^m can be written in the exponential form $\exp(mH_r)$ at and near resonance without divergence difficulties. Finally, there is again an effective Hamiltonian h_r corresponding to H_r that is given in this case by the formula

$$h_r = (\delta/w)f_2 + (\delta/w)F_2\{1 - \exp[-m(\delta/w)F_2]\}$$
$$\times \{1 + \exp[-F_2] + \exp[-2F_2] + \ldots + \exp[-(m-1)F_2]\}f_b + \ldots. \tag{29}$$

Upon inserting (22) into (29), one finds

$$h_r = -2\pi\delta a + c_o(a) + 2\sum_1^\infty c_n(a)[2n\pi\delta/\sin(2n\pi w)]\cos[2n(\Phi + \pi w)]. \tag{30}$$

It is evident that the expression for h_r is well behaved nearby and exactly at the resonance value $\delta = 0$.

As a specific example, consider the case of fourth order resonances. Near a one-quarter tune k = 1, N = 2, and

$$w = 1/4 + \delta. \tag{31}$$

Thus one finds for small δ that

$$\begin{aligned} 2n\pi\delta/\sin 2n\pi w &= 2n\pi\delta/\sin(n\pi/2 + 2n\pi\delta) \\ &= 0(\delta) \text{ for n odd} \\ &= (-1)^{n/2} + 0(\delta^2) \text{ for n even.} \end{aligned} \tag{32}$$

Consequently, neglecting terms of order δD and δ^2, one has in this case for h_r the expression

$$h_r = -2\pi\delta a + c_o(a) + 2\sum_{n \text{ even}} (-1)^{n/2} c_n(a) \cos[2n(\Phi + \pi w)]. \tag{33}$$

Because $-h_r$ acts as an effective Hamiltonian, the fixed points of M^4 are the equilibrium points of h_r. These points are therefore the solutions to the equations

$$0 = \partial h_r/\partial a = -2\pi\delta + c_o'(a) - 2c_2'(a) \cos 4(\Phi + \pi w) + \ldots \tag{34a}$$

$$\begin{aligned} 0 = \partial h_r/\partial \Phi &= 8c_2(a) \sin 4(\Phi + \pi w) \\ &\quad - 16c_4(a) \sin 8(\Phi + \pi w) + \ldots. \end{aligned} \tag{34b}$$

The solutions to (34b) are readily found to be

$$\Phi + \pi w = 0, \pi/4, 2\pi/4, \ldots, 7\pi/4. \tag{35a}$$

When these solutions are inserted into the "radial" Eq. (34a), it takes the simple form

$$0 = -2\pi\delta + c_o'(a) \pm 2c_2'(a) + 2c_4'(a) + \ldots. \tag{35b}$$

Thus, as expected, there are 8 fourth-order fixed points when the tune is near a quarter.

The nature of these fixed points can be obtained by expanding h_r about them. At the fixed points one finds the results

$$\begin{aligned} \partial^2 h_r/\partial a^2 &= c_o''(a) \pm 2c_2''(a) + 2c_4''(a) \ldots \\ \partial^2 h_r/\partial a \partial \Phi &= 0 \\ \partial^2 h_r/\partial \Phi^2 &= \pm 32c_2(a) - 128\, c_4(a) + \ldots. \end{aligned} \tag{36}$$

It follows that if the Eq. (36) are dominated by their first terms, then the fixed points are alternately elliptic and hyperbolic (stable and unstable), as also expected,[7] because the quadratic form corresponding to (36) is either definite or mixed.

Note, moreover, that Eq. (36) and all the higher order terms in the Taylor series expansion about a fixed point are linear in the

beam-beam interaction strength. Consequently, for small beam-beam interaction strength, the size and shape of resonant islands and their associated separatrix structure are independent of the beam-beam interaction strength, and are dependent only on their location in phase space. Only the width of the resonance in tune space, i.e., the rate at which various features move as δ is changed, depends on the interaction strength. This latter dependence can be inferred from (34a) and (35b).

III. NUMERICAL RESULTS

A proper study of the usefulness of h and h_r involves the numerical integration of the trajectories that they generate, or at least a determination of their level lines, and a comparison of these results with points generated by iterating M and M^m numerically. Such a comparison has been made in a similar but simpler problem involving the insertion of a short sextupole element into a ring.[2] In that case the quantitative agreement proved to be excellent, and similar agreement is expected for this problem as well.

However, because of the complexity of evaluating the coefficients $c_n(a)$, the equivalent study has not yet been carried out for the present problem. Instead, a preliminary exploration of the nature of M has been made by studying the points obtained by iterating M numerically. In this section it will be shown that M indeed does have all the qualitative properties that were predicted in the previous section.

Figures 2 through 5 show phase-space plots generated by successive iterates of M for various initial conditions and tune values. The phase-space coordinates range over (-2, 2), and the scale is chosen so that the beam lies within (-1, 1).[1] The tunes are near the resonant values 1/2, 1/4, 1/6, and 1/8 respectively, and the beam-beam interaction strength is 10^{-2}. Observe that the size of resonance features, e.g., island dimensions, indeed do decrease with increasing order of the resonance. Symmetry about the line $\phi = \pi/2 - \pi w$ and inversion symmetry are evident. The number and nature of fixed points is as anticipated.

Figure 6, which appears to be almost identical to Fig. 3, was obtained by running at a tune w = 0.253 and a beam-beam interaction strength of 5×10^{-3}. It shows, as predicted, that the size of resonant features is independent of the size of the interaction strength provided the tune is suitably adjusted so as to make the features appear in the same region of phase space. Note that according to (35b), when the size of the c_n is halved, δ should also be halved to keep the radial location of fixed points the same. Examination of the tune values for Figs. 3 and 6 shows that this is indeed the case. When the tune is thus adjusted, there is a slight change in the angular location of the fixed points in accord with (35a).

Figure 7 shows a tenth-order resonance obtained by running near a tune of 1/10. It was not shown as part of the sequence of Figs. 2 through 5 because the island structure becomes too small to see when (by adjusting the tune) it is located closer to the origin. This example verifies that the sizes of resonant features decrease with proximity to the origin, and in fact the higher the order of the

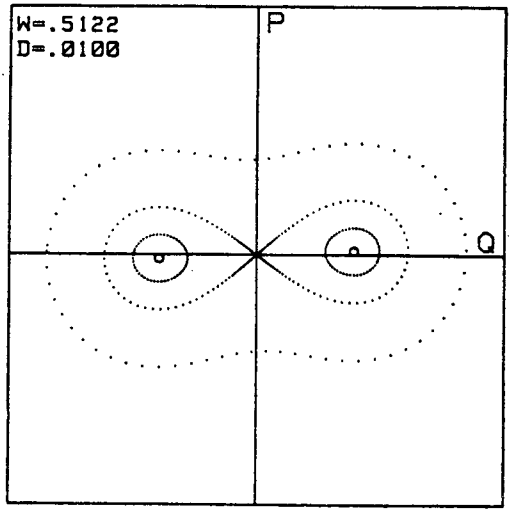

Fig. 2. Phase-space plot generated by successive iterations of the transfer map M for various initial conditions. The tune is near one half. The coordinates extend from - 2 to 2, and are normalized in such a way that the beam will be within the unit circle under actual operating conditions. The beam-beam interaction strength is 10^{-2}.

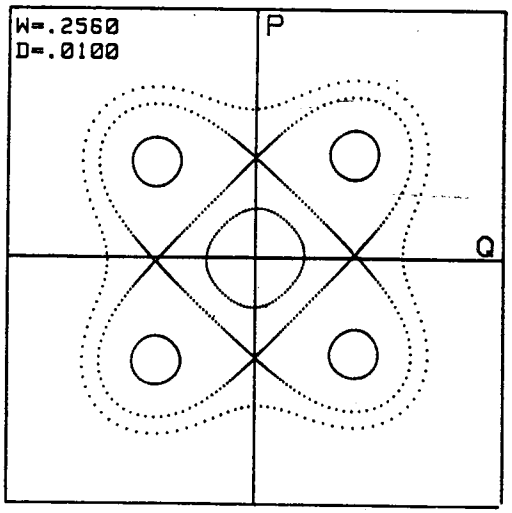

Fig. 3. Phase-space plot when the tune is near one fourth.

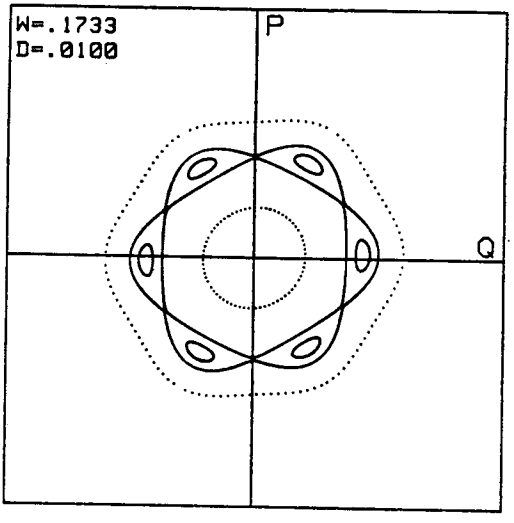

Fig. 4. Phase-space plot when the tune is near one sixth.

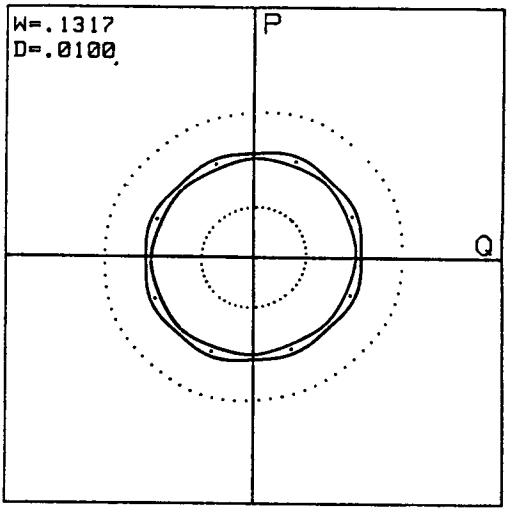

Fig. 5. Phase-space plot when the tune is near one eighth.

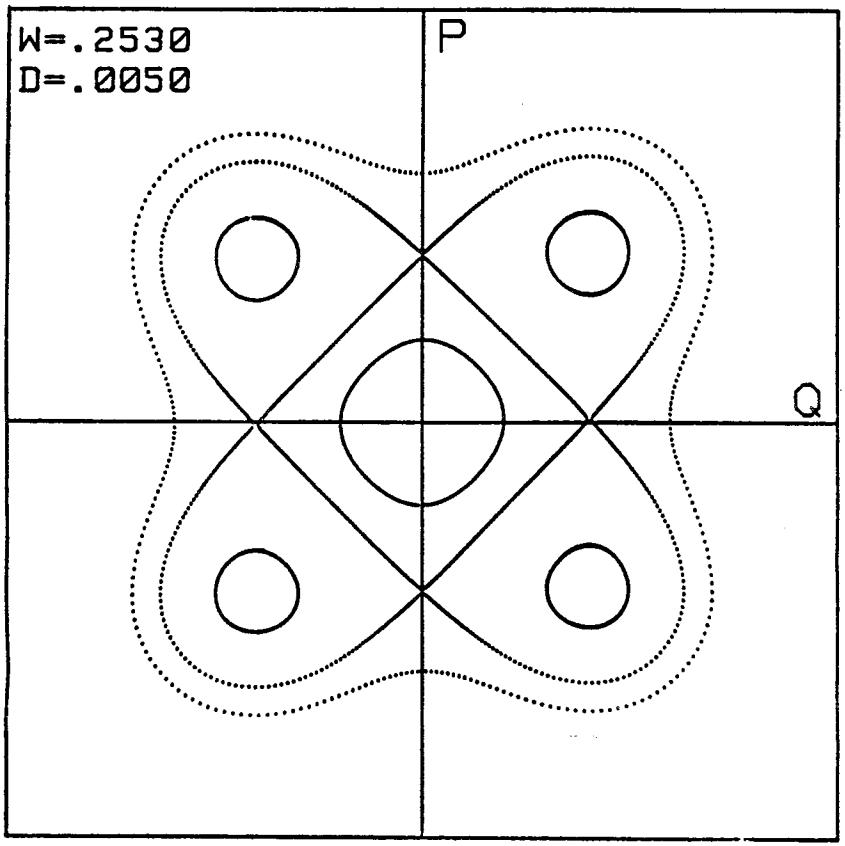

Fig. 6. Phase-space plot when the interaction strength is half that of Fig. 3. The initial p, q values are the same as in Fig. 3, and the tune is adjusted to make various phase-space features match those in Fig. 3.

resonance, the more rapid is the decrease.

Figure 8 shows the result of running with a nonresonant tune of 77/100. On the scale shown and for the number of iterations made, there seems to be no evidence that any points will leave the beam envelope. The nature of the map and any tendency for points to move off what appear to be invariant curves could be examined in finer detail by studying the value of h(z) at each point. Because h generalizes the Courant-Snyder invariant, its variations could be used as a kind of "magnifying glass" to give evidence for small scale homoclinic or stochastic behavior that is not otherwise discernible to the naked eye and that might lead to eventual particle loss. This method has been used to show that particle motion in the Van Allen radiation belts is not integrable.[8]

Figure 9 illustrates that stochastic behavior indeed can occur for the beam-beam problem if the interaction strength is large enough and the tune (taking into account its depression by the beam-beam

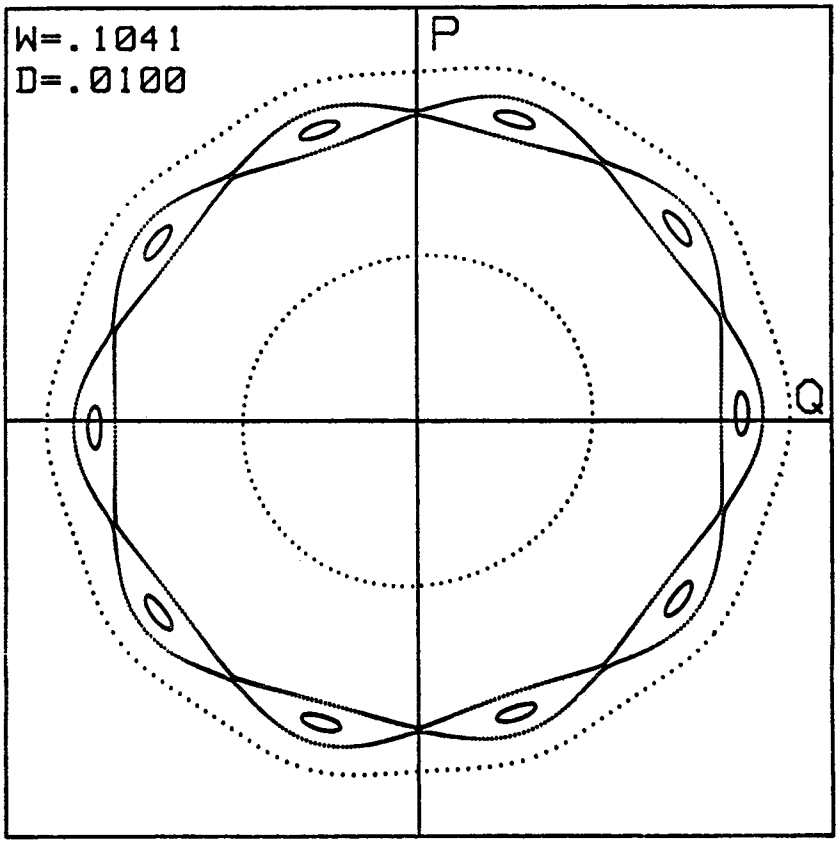

Fig. 7. Phase-space plot near a tune of one tenth.

interaction) is sufficiently close to a resonant value. The stochastic behavior in this case leads to particle losses within a few hundred turns.

IV. CONCLUDING REMARKS AND COMMENTS

Operation of ISABELLE with each 1/6 lattice section having a tune near a multiple of 1/2, 1/4, 1/6, or 1/8 corresponds to operating the total ring near an integer, half integer, or quarter integer tune. Because operation of the total ring near any of these tunes is probably already precluded by structure resonances in the ring, the first beam-beam interaction resonance of significance is at least of tenth order. Figure 7 illustrates that the tenth-order resonance structure is small even when it is far from the phase-space origin, and consequently it is even smaller when it is within the beam. This observation, and the regular behavior found in the nonresonant case of Fig. 8, give preliminary evidence that within the model employed, the beam-beam interaction at its contemplated strengths should not lead to particle loss. However, in accord with our earlier comment, it would be worthwhile to examine the behavior of $h(z)$ and $h_r(z)$ for evidence of small scale stochastic behavior.

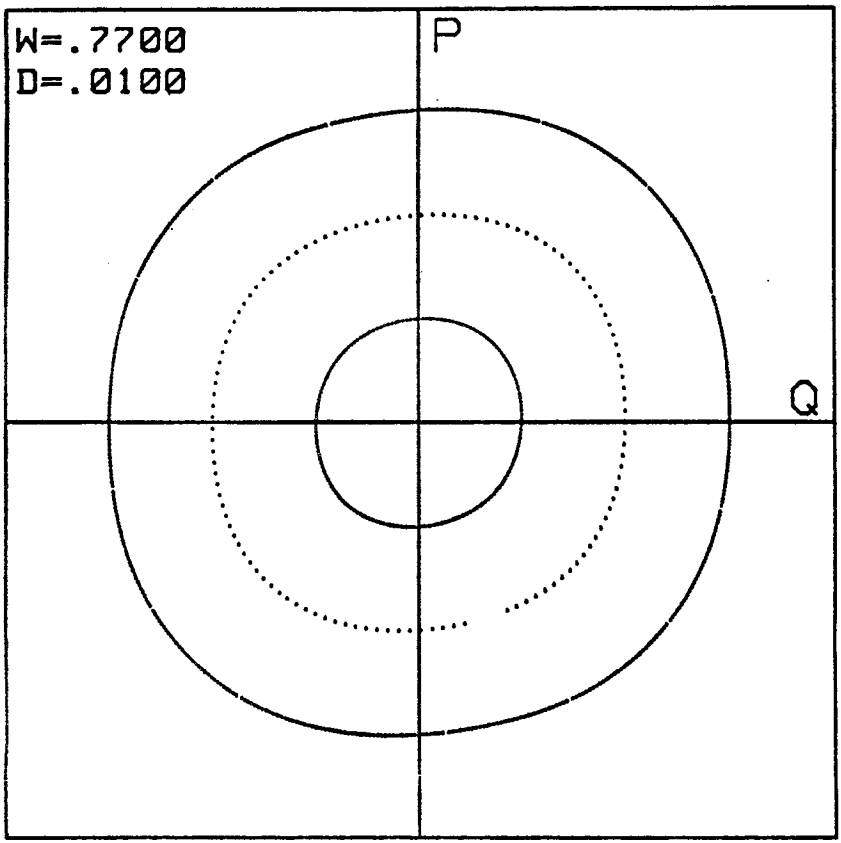

Fig. 8. Phase-space plot for a nonresonant tune.

The conclusion that resonances below tenth order are not significant depends on the assumption that all 6 interaction regions and all 6 lattice periods are identical. The validity of this assumption should be examined, and the effect of lower order resonances should be reexamined when the 6 interaction regions are all slightly different.

Finally, consideration should be given to the possible effect of adding nonlinearities to the transfer map for the ring. It is anticipated that the addition of suitable nonlinearities, perhaps by the use of octupoles, would lead to a reduction in the size of beam-beam interaction resonance structures. In particular, it would then no longer be the case that the size of resonant structures would depend only on their location in phase space and not on the interaction strength. It might turn out, of course, that the ring nonlinearities required to achieve a significant effect would be difficult to obtain or would be undesirable for other reasons.

ACKNOWLEDGMENT

The author wishes to thank Dr. Richard K. Cooper for many helpful conversations.

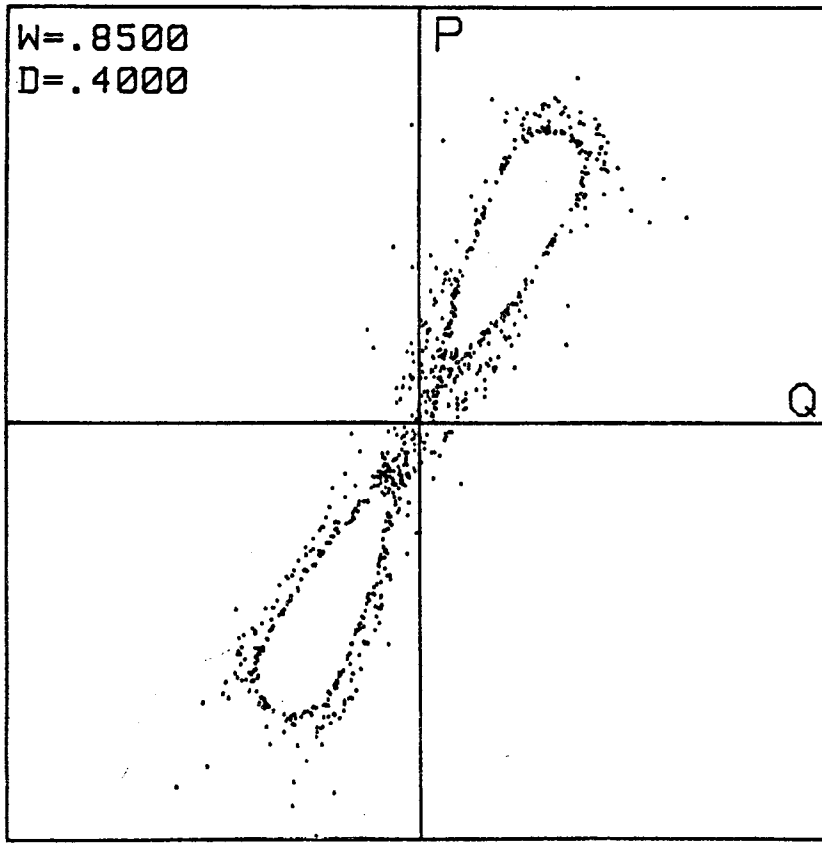

Fig. 9. Phase-space plot showing stochastic behavior for large beam-beam interaction strength. The reader is invited to draw the symmetry line $\hat{\varphi} = \pi/2 - \pi w$.

REFERENCES

1. J. C. Herrera, M. Month, and R. F. Peierls, Brookhaven National Laboratory Report BNL 25703 (1979).
2. A. Dragt, "A Method of Transfer Maps for Linear and Nonlinear Beam Elements," To appear in IEEE Transactions on Nuclear Science, NS 26 (1979).
3. A. Dragt and J. Finn, J. Math. Phys. 17, pp. 2215-2227 (1976).
4. J. C. Herrera, Brookhaven National Laboratory Report BNL 25703 (1979).
5. M. Abramowitz and I. Stegun, Eds., Handbook of Mathematical Functions, National Bureau of Standards Applied Mathematics Series 55 (1966).
6. S. Sternberg, Celestial Mechanics, part II, (W. A. Benjamin, New York, 1969), p. 18.
7. V. Arnold and A. Avez, Ergodic Problems of Classical Mechanics, (W. A. Benjamin, New York, 1968).
8. A. Dragt and J. Finn, J. of Geophys. Res. 81, pp. 2327-2339 (1976).

energetic charged particles, mostly electrons, from the nuclear explosions [*Hess* 1964*b*]. These seven explosions are shown in Table 3. The Argus explosions were

TABLE 3. High-Altitude Nuclear Explosions That Have Produced Artificial Radiation Belts

Explosion	Locale	Time	Yield	Altitude
Argus 1	South Atlantic	August 27, 1958	1 kt	~300 miles
Argus 2	South Atlantic	August 30, 1958	1 kt	~300 miles
Argus 3	South Atlantic	September 6, 1958	1 kt	~300 miles
Starfish	Johnston Island, Pacific Ocean	July 9, 1962	1.4 Mt	400 km
USSR	Siberia	October 22, 1962	Several hundred kt	?
USSR	Siberia	October 28, 1962	?	?
USSR	Siberia	November 1, 1962	?	?

performed to study the trapping of particles in the earth's magnetic field. *Christofilos* [1959] had suggested that electrons from β decay of fission fragments from a nuclear explosion should be able to make an artificial radiation belt. All seven artificial belts to date are from this source. The Argus belts, studied by *Van Allen et al.* [1959*b*] on Explorer 4, decayed in about a week. During this time they did not move radially a measurable amount.

The Starfish explosion made a much more extensive belt than Argus. Electron fluxes as large as 10^9 cm^{-2} sec^{-1} were produced. The belt was studied at early times by detectors on Injun 1 [*O'Brien et al.*, 1962*a*], Traac [*Pieper et al.*, 1963], Te-

their time histories. All these belts decayed rapidly, as did the Starfish belt for $L > 1.7$. The short lifetime at high altitude is very probably due to some type of electromagnetic waves interacting with the electrons. *Dungey* [1963] and *Cornwall* [1964] have suggested that whistlers, circularly polarized waves that travel

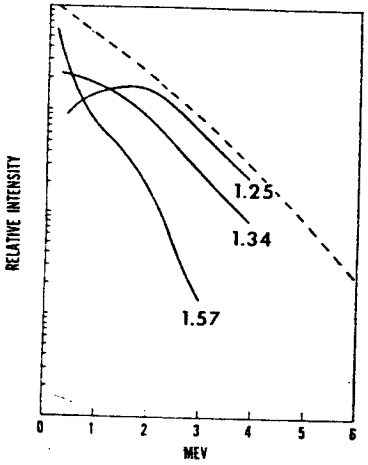

Fig. 20. Energy spectrums of electrons in the Starfish artificial radiation belt as measured on satellite 1962βk. The three curves are at *different* L values.

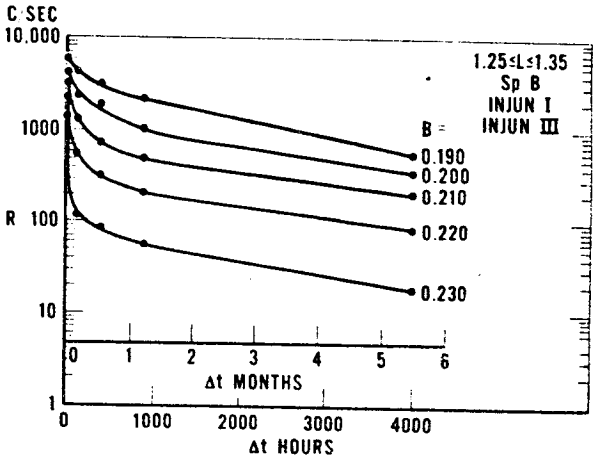

Fig. 21. Decay of the Starfish artificial radiation belt electrons at low altitudes as measured on Injun.

Advances in Particles and Field Research in the Satellite Era

W. N. HESS, G. D. MEAD AND M. P. NAKADA

Goddard Space Flight Center, Greenbelt, Maryland

Abstract. The last six years have seen a rapid progress in the exploration of extraterrestrial phenomena. This paper gives a survey of the more important results from investigations of energetic particle radiations, plasmas, and magnetic fields in space. One of the highlights of these investigations was the discovery and study of the continuous flow of plasma away from the sun, the so-called solar wind. This plasma flow confines the earth's magnetic field within about 10 R_E on the day side and is responsible for the magnetospheric tail, which is thought to extend beyond the orbit of the moon. Inside this cavity, large fluxes of magnetically confined energetic charged particles were discovered. Confinement lifetimes in the tail have not yet been established; however, out to roughly 8 R_E the particles are trapped and constitute the Van Allen radiation belt. The study of the solar cosmic rays that accompany some solar flares is enhancing our understanding of solar processes and of the interplanetary medium through which the solar protons travel. Continued investigations of cosmic rays are leading to a better knowledge of the heavy particle component, of the low-energy end (below 100 Mev) of the spectrum, and of the processes responsible for Forbush decreases. On the basis of these discoveries, a new picture is emerging of our environment and, more generally, of the processes in the solar system.

1. INTRODUCTION

Before the satellite era, there was relatively little knowledge of the environment of the earth above 100 km. The existence of the ionosphere was known originally from a study of radio waves and later from direct observations by balloons and rockets. Measurements of the zodiacal light had indicated that there were electrons through all space near the sun, but it was quite uncertain how many electrons there were and in what fashion they were moving. From a knowledge of the earth's surface magnetic field the field could be predicted some distance into space. From this information a crude picture of near-earth space developed, which we now know to be very incomplete and to a certain extent mistaken. The first U. S. satellite revised in a dramatic way our picture of the environment.

The first indication of the existence of geomagnetically trapped radiation came early in 1958 with the launching of Explorers 1 and 3. Van Allen observed an anomalously high counting rate, followed by a period of zero count rate due to saturation of the Geiger counter as the satellite entered the radiation belt. These first experiments were followed by innumerable others that confirmed the existence of two broad zones of penetrating particles: an inner zone consisting primarily of protons and an outer zone consisting predominantly of electrons. The composition, energy spectrums, and temporal and spatial variation of these belts have been extensively studied by satellites and space probes. In addition, a series of United States and Russian nuclear explosions in space has demonstrated the possibility of producing long-lived artificial radiation belts.